Development/Plasticity/Repair

Cholinergic-Mediated IP_3-Receptor Activation Induces Long-Lasting Synaptic Enhancement in CA1 Pyramidal Neurons

David Fernández de Sevilla,[1] Angel Núñez,[2] Michel Borde,[1] Roberto Malinow,[3] and Washington Buño[1]

[1]Instituto Cajal, Consejo Superior de Investigaciones Científicas, 28002 Madrid, Spain, [2]Departamento de Anatomía, Histología y Neurociencia, Facultad de Medicina, Universidad Autónoma de Madrid, 28029 Madrid, Spain, and [3]Cold Spring Harbor Laboratory, Cold Spring Harbor, New York 11724

Cholinergic–glutamatergic interactions influence forms of synaptic plasticity that are thought to mediate memory and learning. We tested *in vitro* the induction of long-lasting synaptic enhancement at Schaffer collaterals by acetylcholine (ACh) at the apical dendrite of CA1 pyramidal neurons and *in vivo* by stimulation of cholinergic afferents. *In vitro* ACh induced a Ca^{2+} wave and synaptic enhancement mediated by insertion of AMPA receptors in spines. Activation of muscarinic ACh receptors (mAChRs) and Ca^{2+} release from inositol 1,4,5-trisphosphate (IP_3)-sensitive stores were required for this synaptic enhancement that was insensitive to blockade of NMDA receptors and also triggered by IP_3 uncaging. Activation of cholinergic afferents *in vivo* induced an analogous atropine-sensitive synaptic enhancement. We describe a novel form of synaptic enhancement (LTP_{IP3}) that is induced *in vitro* and *in vivo* by activation of mAChRs. We conclude that Ca^{2+} released from postsynaptic endoplasmic reticulum stores is the critical event in the induction of this unique form of long-lasting synaptic enhancement.

Key words: **LTP_{IP3}; endoplasmic reticulum; Ca^{2+} wave; AMPA trafficking; inositol; muscarinic**

Introduction

Activity-dependent long-term modifications in synaptic efficacy are thought to be the cellular basis of memory and learning, but the causal mechanisms of these synaptic changes are still controversial and more diverse than previously considered. Insufficiently explored examples are the interactions between different neurotransmitter systems in synaptic plasticity. Cholinergic–glutamatergic interactions can influence forms of synaptic plasticity in the hippocampus (Aigner, 1995; Ovsepian et al., 2004) that may underlie cognitive processes (Blokland, 1995; Hasselmo, 1999; Shinoe et al., 2005), and lesions of the septohippocampal cholinergic projections produce cognitive deficits. Septohippocampal afferents release acetylcholine (ACh) and trigger the hippocampal theta rhythm (Dudar, 1977) that has been related to learning and memory (Huerta and Lisman, 1995; Hoffman et al., 2002). Protracted activation of muscarinic ACh receptors (mAChRs) may induce increases in glutamatergic synaptic efficacy (Auerbach and Segal, 1994, 1996), suggesting that cholinergic activity may be central in memory encoding (Hasselmo, 1999).

The production of inositol 1,4,5-trisphosphate (IP_3) induced by mAChR activation triggers the major mechanism of Ca^{2+} release from endoplasmic reticulum (ER) stores in CA1 pyramidal neurons (Power and Sah, 2002). M1 and M3 mAChRs are coupled to phospholipase C (PLC) and via heterotrimeric G-protein (G_q/11) hydrolyze phosphatidylinositol 4,5-bisphosphate, producing IP_3 and diacylglycerol (Abe et al., 1992). IP_3 activates IP_3 receptors (IP_3Rs) that induce Ca^{2+} release from IP_3-sensitive ER stores. The rise in intracellular Ca^{2+} may regulate a number of processes, including synaptic plasticity (Rose and Konnerth, 2001; Bardo et al., 2006), that are thought to occur in dendritic spines, as was initially advanced by Ramón y Cajal (1891).

Because a rise in postsynaptic Ca^{2+} can lead to synaptic enhancement (Zucker, 1999; Rose and Konnerth, 2001), we tested the synaptic effects *in vitro* of a brief local application (puff) of the natural transmitter ACh at the apical dendrites of CA1 pyramidal cells and of *in vivo* activation of septohippocampal cholinergic afferents. We report that ACh induced both a slow Ca^{2+} wave that propagates along the apical dendritic shaft and a long-lasting enhancement of Schaffer collateral (SC) EPSCs. Activation of M1 mAChRs and release of Ca^{2+} from IP_3-sensitive stores are required to induce this long-lasting synaptic enhancement that we called $LTP_{IP3.}$ LTP_{IP3} is insensitive to block of NMDA receptors (NMDARs) and is paralleled by an increased expression of AMPA receptors (AMPARs) in spines. This novel IP_3-dependent form of synaptic enhancement requires Ca^{2+} release from ER

Received June 15, 2007; revised Dec. 11, 2007; accepted Dec. 21, 2007.

W.B. and A.N. were supported by Dirección General de Investigación Científica y Tecnológica, Ministerio de Educación y Cultura Grant BFU2005-07486 (Spain). D.F. was initially funded by Ministerio de Ciencia y Tecnología (BFI2002-01107) and Comunidad Autónoma de Madrid Grants GR/SAL/0877/2004 and at present by Ministerio de Ciencia y Tecnología Grant BFU2005-07486. M.B. was on leave from the Departamento de Fisiología, Facultad de Medicina, Universidad de la República, Montevideo, Uruguay. Financial support for R.M. was provided by the National Institutes of Health.

Correspondence should be addressed to David Fernández de Sevilla, Instituto Cajal, Consejo Superior de Investigaciones Científicas, Avenida Dr. Arce 37, 28002 Madrid, Spain. E-mail: desevilla@cajal.csic.es.

DOI:10.1523/JNEUROSCI.2723-07.2008

 0270-6474/08/281469-10$15.00/0

stores without the need of correlated presynaptic–postsynaptic action potentials.

Materials and Methods

Procedures of animal care, surgery, and slice preparation were in accordance with the guidelines laid down by the European Communities Council. The procedures will be described briefly because they have been extensively detailed previously (Borde et al., 1995; Fernandez de Sevilla and Buno, 2003).

Slice preparation. Young Wistar rats (14–16 d of age) were decapitated, and the brain was removed and submerged in cold (~4°C) artificial CSF (ACSF; in mM: 124.00 NaCl, 2.69 KCl, 1.25 KH_2PO_4, 2.00 Mg_2SO_4, 26.00 $NaHCO_3$, 2.00 $CaCl_2$, and 10.00 glucose). The pH was stabilized at 7.4 by bubbling the ACSF with carbogen (95% O_2, 5% CO_2). Picrotoxin (50 μM) was added to the ACSF to block $GABA_A$-mediated inhibition. In these conditions, abnormal epileptiform activity was never observed in our sample. Transverse hippocampal slices (300–350 μm thick) were cut with a Vibratome (Pelco 3000; Pelco, St. Louis, MO) and incubated in the ACSF (>1 h, at room temperature, 20–22°C). Slices were transferred to a 2 ml chamber fixed to an upright microscope stage (BX51WI; Olympus, Tokyo, Japan) equipped with infrared differential interference contrast video microscopy and a 40× water-immersion objective. Slices were superfused with carbogen-bubbled ACSF (2 ml/min) and maintained at room temperature. In some cases, experiments at higher temperatures in the more physiological range of 32°C were also performed. DL-2-Amino-5-phosphonovaleric acid (APV; 50 μM), 6-cyano-7-nitroquinoxaline-2,3-dione (CNQX; 20 μM), (+)-α-methyl-4-carboxyphenylglycine (MCPG; 1 mM), atropine (0.3 μM), pirenzepine (75 nM), methoctramine (1 μM), methyllycaconitine (MLA; 0.1 μM; in some cases, higher doses of MLA, up to 125 μM, were used), thapsigargin (1 μM), and tetrodotoxin (TTX; 100 nM) were added to the ACSF as needed. Thapsigargin was dissolved in DMSO (0.01%). DMSO at the final concentrations used had no effects on synaptic responses or postsynaptic conductances ($n = 3$).

Recordings and analysis. Whole-cell recordings from soma of CA1 pyramidal cells were performed with patch pipettes (4–8 MΩ) filled with an internal solution that contained (in mM) 135 K-$MeSO_4$, 10 HEPES, 0.2 EGTA, 2 Na_2-ATP, and 0.4 Na_3-GTP, buffered to pH 7.2–7.3 with KOH. In some experiments, the intracellular solutions contained heparin (5 mg/ml), ruthenium red (400 μM), or 1,2-bis (*o*-aminophenoxy) ethane-*N*,*N*,*N*′,*N*′-tetraacetic acid (BAPTA; 50 mM). Recordings were performed in the voltage-clamp mode using a Cornerstone PC-ONE amplifier (DAGAN, Minneapolis, MN). Pipettes were placed with a hydraulic micromanipulator (Narishige, Tokyo, Japan). The holding potential (V_h) was adjusted to −60 mV, and the series resistance was compensated to ~80%. Neurons were accepted only when the seal resistance was >1 GΩ and the series resistance (10–20 MΩ) did not change >10% during the experiment. Data were high-pass filtered at 3.0 kHz and sampled at 10.0 kHz, through a Digidata 1322A (Molecular Devices, Sunnyvale, CA). The pClamp programs (Molecular Devices) were used to generate stimulus timing signals and transmembrane current pulses, and to record and analyze data. EPSCs were evoked by stimulation of SC with a nichrome bipolar electrode (60 μm diameter; tip separation, ~100 μm) placed in the stratum radiatum ~100–200 μm from the soma of the recorded neuron. A Grass S88 and SIU (Quincy, MA) generated the stimulation pulse protocols. Stimulation intensity was adjusted to evoke EPSC amplitudes between 30 and 60 pA. Brief, localized, ACh puffs (300 ms duration) were applied through a pipette (tip diameter, ~5 μm) loaded with ACh (1 mM) and connected to a Picospritzer II (General Valve, Fairfield, NJ). The pipette tip was placed during the puff with a hydraulic micromanipulator (Narishige) close (~20–50 μm) to the apical dendritic shaft ~20 μm from the soma of the recorded CA1 pyramidal neuron and withdrawn from the tissue immediately after the puff. Chemicals were purchased from Sigma-Aldrich Química (Madrid, Spain), Tocris Bioscience (Ellisville, MO; distributed by Biogen Científica, Madrid, Spain), and Alomone Labs (Jerusalem, Israel).

Ca^{2+} imaging and photolysis of caged IP_3. Simultaneous electrophysiology recordings and intracellular Ca^{2+} imaging were obtained. The latter was performed by fluorescence microscopy with the Ca^{2+} indicator fluo-3 (Invitrogen, Eugene, OR). Patch pipettes were filled with the internal solution containing 50–100 μM fluo-3. Imaging experiments were performed after a 10–15 min stabilization period that allowed the equilibration of the dye in the soma and apical dendritic shaft. Cells were illuminated during 40 ms every 200 ms at 490 nm with a monochromator (Polychrome IV; TILL Photonics, Planegg, Germany), and successive images were obtained at 5 s^{-1} with a cooled monochrome CCD camera (Cohu 4920; San Diego, CA) attached to the Olympus microscope that was equipped with a filter cube (Chroma Technology, Rockingham, VT) optimized for fluo-3. Camera control, synchronization with electrophysiological measurements, and quantitative epifluorescence measurements were made with the ImagingWorkbench software (INDEC-BioSystems, Santa Clara, CA). Changes in fluorescence signals were expressed as the proportion (percentage) of relative change in fluorescence ($\Delta F/F_0$), where F_0 is the prestimulus fluorescence level when the cell is at rest and ΔF is the change in fluorescence during activity. Plots of Ca^{2+} signal variations versus time were obtained "off-line" at specified regions of interest from stored image stacks and expressed as $\Delta F/F_0$. Corrections were made for indicator bleaching during trials by subtracting the signal measured under the same conditions when the cell was not stimulated. The off rate of fluo-3 is fast enough to detect Ca^{2+} decay time constants of ~80 ms (Markram et al., 1995), which are well below those measured in our experiments. Therefore the differences in decay time course between the Ca^{2+} signals reported in Results should reflect differences in Ca^{2+} decay rates.

Flash photolysis of caged IP_3 was performed after filling pyramidal neurons with a pipette solution that contained fluo-3 and caged IP_3 (Calbiochem, La Jolla, CA) at 100 μM. The cell was illuminated with a flash unit (UV Flash II; TILL Photonics) attached to the microscope through a dual port condenser, and simultaneous electrophysiological recordings and Ca^{2+} imaging were carried out.

An average baseline of control EPSCs was obtained by repeated stimulation at 0.3 Hz, and the magnitude of the average changes in peak EPSC amplitude induced by the various procedures tested were expressed as a proportion (percentage) of the baseline control amplitude and plotted as a function of time. Statistical estimations were performed with the maximum peak EPSC values in the course of the LTP_{IP3} and when the EPSC amplitude had attained a steady state (30 min after the LTP_{IP3} induction). The presynaptic or postsynaptic origin of the changes in EPSC amplitude was estimated using the paired-pulse ratio (PPR; R2/R1), where R1 and R2 were the average peak amplitudes of the first and second EPSCs, respectively (Fernandez de Sevilla et al., 2002). Statistical analysis was performed using the Origin 7.0 program (OriginLab, Northampton, MA).

Analysis of AMPAR trafficking. The super-ecliptic pHluorin (SEP) coding sequence was inserted three amino acids downstream of the predicted signal peptide cleavage site of the corresponding AMPAR subunit. The red fluorescent protein (tDimer dsRed) is a fast maturing obligate dimer version of dsRed. We generated a Sindbis virus with a double promoter that drives expression of GluR-SEP and tDimer dsRed. We infected CA1 pyramidal neurons *in vivo* by injecting Wistar rats (12 d of age) with GluR1-SEP- and GluR2-SEP-expressing Sindbis viruses (both viruses also expressing tDimer dsRed) and allowed to express for 36–48 h. Then the animals were killed, and transverse slices were obtained as described above.

Two-photon laser-scanning microscopy high-resolution three-dimensional image stacks were collected on a custom-built instrument based on a Fluoview laser-scanning microscope (Olympus America, Melville, NY). The light source was a mode-locked Ti:sapphire laser (Mira 900F; Mira, Santa Clara, CA) running at 910 nm. We used a LUMPlanFl/IR 40× 0.80 numerical aperture objective. Each optical section was resampled three times and was captured every 0.5 μm. Two full stacks were captured (at −10 and 0 min) before LTP_{IP3} induction and two more stacks at 30 and 60 min after induction of LTP.

Spines were analyzed using custom software written in MatLab (The MathWorks, Natick, MA) and identified using the tDimer channel. Rectangular regions of interest were manually positioned to fully cover each spine. Individual spines were numbered and followed in a time-lapse recording. When the identity of a protrusion was unclear (for instance, two spines appear as one), the specific spine was not included in the

analysis. In addition, no effort was made to analyze spines emerging below or above the dendrite, because the two-photon excitation laser-scanning microscopy resolution of these is compromised. Dendrite regions of interest were placed at the base of each spine centered on the dendrite with approximately the same area as the corresponding spine regions of interest. Total integrated fluorescence (in arbitrary units) for both green and red channels was computed for each section in a stack. Background and spillover (from the other channel) fluorescence were subtracted to generate a background- and spillover-subtracted integrated fluorescence value for each channel as a function of depth. The potential effects of Forster resonance energy transfer (FRET) between SEP and tDimer were not compensated given the highly unlikely occurrence of FRET across a membrane between no linked fluorophores. For dendrites, the mean pixel fluorescence (rather than integrated fluorescence) was taken within these boundaries to negate any effect that alterations in the size of the selected region would have. Enrichment of receptors on spines was defined as (Spine green/Spine red)/(Dendrite green/Dendrite red); this fluorescence ratio is used as a relative, not absolute, means of determining enrichment.

In vivo *experiments.* Data were obtained from 18 urethane-anesthetized (1.6 g/kg, i.p.) young adult Wistar rats (between 3 and 4 months of age) of either sex, weighing 180–250 g. Animals were placed in a stereotaxic device. The body temperature was maintained at 37°C, and the end-tidal CO_2 concentration was monitored. Experiments were performed in accordance with the European Communities Council Directive (86/609/EEC). Extracellular recordings were with tungsten macroelectrodes (1 MΩ) implanted in the CA1 region [anterior (A), −2.3; lateral (L), 1; vertical (V), 2.5 mm from bregma]. SC fibers were stimulated using a bipolar stainless steel stimulating electrode (0.1 mm diameter) placed in the stratum radiatum (A, −2.3; L, 4; V, 4 mm from bregma). The medial septum (A, −0.2; L, 0; V, 7 mm from bregma) was also stimulated using a similar bipolar electrode. Electrodes were placed stereotaxically according to the Paxinos and Watson (1986) atlas. Extracellular excitatory postsynaptic field potentials (fEPSPs) were recorded in the CA1 layer. fEPSPs were amplified (AC amplifier; World Precision Instruments, Sarasota, FL), bandpass filtered between 0.1 Hz and 1.0 kHz, and digitized at 3.0 kHz (CED 1401 with Spike 2 software; Cambridge Electronic Design, Cambridge, UK). A control baseline fEPSP was obtained with single-pulse stimulation (100 μA, 0.3 ms, 0.5 Hz) applied at the SCs during 4 min. fEPSP averages ($n = 15$) were calculated every 60 s, and the slope of the initial phase was taken as an estimation of the magnitude of the fEPSP. Data was presented as the proportion of changes (100%) relative to the mean control baseline fEPSP slope calculated throughout the initial 4 min. Recordings were accepted for analysis when baseline variability was <10%. The high-frequency stimulation (HFS) of the medial septum used to induce long-term potentiation (LTP) consisted of three 500 ms duration pulse barrages of 100 μA, 0.3 ms pulses at 100 Hz presented every 2 s delivered without SC stimulation. The stimulation frequency of 100 Hz is similar to the discharge rate exhibited by groups of medial septal neurons (Gaztelu and Buno, 1982; Zenchenko et al., 2000), suggesting that high firing rate activity could be present in physiological conditions.

Recording was maintained for 60 min after the tetanic stimulation. Similar recordings were performed in control conditions and after intraperitoneal injection of atropine sulfate (5 mg/kg). Chemicals were purchased from Sigma-Aldrich Química.

Statistical analysis. Results are given as mean ± SEM (n = number of cells or number of experiments in extracellular recordings), and percentages are presented as percentage of controls. Statistical analyses were calculated with Student's two-tailed t tests for unpaired or paired data as required. The threshold level of significance was set at $p < 0.05$ (*); $p < 0.01$ (**), and $p < 0.001$ (***).

Results

ACh induces a postsynaptic Ca^{2+} elevation and long-lasting synaptic enhancement

A brief ACh puff (300 ms duration) applied at the apical dendritic shaft (~20 μm from the soma) induced an EPSC inhibition (a 48.5 ± 9.5% peak amplitude reduction; $p < 0.001$; lasting 2.1 ± 0.8 min; $n = 20$), caused by mAChR-mediated blockade of N-type Ca^{2+} channels at SC terminals (Valentino and Dingledine, 1981; Qian and Saggau, 1997). This presynaptic inhibition was paralleled by a long-lasting inward current (Fig. 1*A*) caused by the suppression of several potassium conductances mediated by postsynaptic mAChRs (Dutar and Nicoll, 1988). These initial effects of ACh were followed by a strong and sustained increase in EPSC peak amplitude or LTP_{IP3} (a 205.5 ± 14.0% increase; $p < 0.001$; same cells) (Fig. 1*A*). The magnitude of the presynaptic inhibition was essentially identical to that obtained by electrical

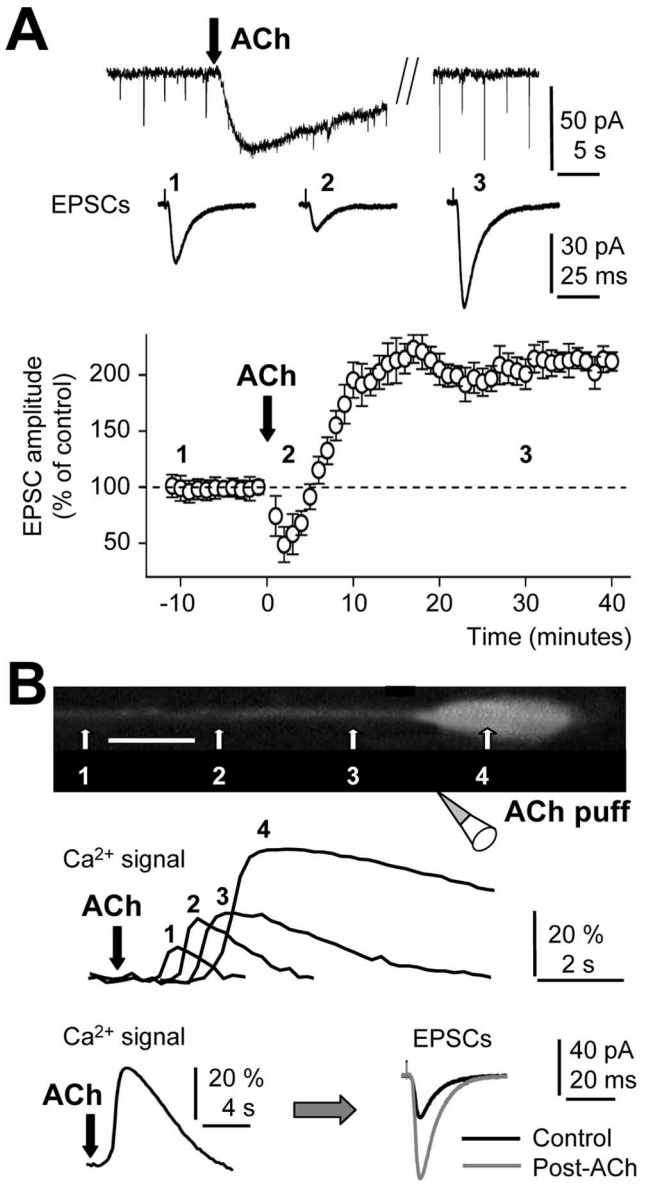

Figure 1. ACh induces a Ca^{2+} wave and long-lasting synaptic enhancement. ***A***, Top, Representative EPSCs (brief inward deflections) and inward current induced by ACh application. ***A***, Middle, Representative averaged EPSCs ($n = 20$; as in all other cases) before (1) and during synaptic inhibition (2) and enhancement (3) induced by ACh application. ***A***, Bottom, Time course of the EPSC amplitude (percentage) during the induction of LTP_{IP3} by ACh (black arrow; $n = 20$). ***B***, Top, Representative CA1 pyramidal neuron loaded with fluo-3 (100 μM) and the superimposed Ca^{2+} signals recorded at four different sites in the dendrite (white arrows 1, 2, 3, and 4). Note that the fluorescence signal originates in the distal part of the dendrite (1) and increases as it spreads to the soma (4). Scale bar, 35 μm. ***B***, Bottom, Averaged somatic Ca^{2+} signal induced by ACh and superimposed EPSCs before (Control; black trace) and after ACh (30 min after ACh as in all other figures; gray trace) showing the potentiation.

stimulation of hippocampal cholinergic afferent fibers, suggesting that the ACh puff activated a group of receptors similar to that activated by the more physiological afferent stimulation (Fernandez de Sevilla and Buno, 2003).

Simultaneous electrophysiology and Ca^{2+} imaging revealed that the ACh puff was followed at brief delays (1.9 ± 0.2 s; $n = 20$) by a strong increase of the intracellular Ca^{2+} signal ($39.5 \pm 5.2\%$; $n = 20$ measured at the soma) that occurred in parallel with the presynaptic inhibition and with the initial portion of the long-lasting inward current. The Ca^{2+} elevations induced by the ACh puffs always preceded (6.2 ± 2.6 min) the onset of the synaptic enhancement (Fig. 1*B*, Control), started distally in the apical dendrite, usually at the first branch point far (~ 150 μm) from the ACh application site, and rapidly propagated to the soma at a constant speed of $\sim 100.5 \pm 20.7$ $\mu m \cdot s^{-1}$ ($n = 20$) (Fig. 1*B*; see supplemental video 1, available at www.jneurosci.org as supplemental material). The Ca^{2+} signal gradually increased in duration on its way to the soma (analyzed from similar areas of interest along the apical dendritic shaft and soma). The Ca^{2+} signal in the apical dendrite ~ 150 μm from the soma had a $\Delta F/F_0$ of $10.5 \pm 2.1\%$ and lasted 1.5 ± 0.2 s ($n = 20$), whereas the large prolonged somatic Ca^{2+} signal had a $\Delta F/F_0$ of $39.5 \pm 5.2\%$ and lasted 10.2 ± 2.0 s (same cells). The mean total duration of the Ca^{2+} signal from its onset at the dendritic branch point to its termination at the soma was $13.8. \pm 2.6$ s (same cells) (Fig. 1*B*).

The postsynaptic Ca^{2+} elevation and long-lasting synaptic enhancement require activation of M1 mAChR

Activation of mAChRs may facilitate the induction of LTP with conventional stimulation protocols, and forms of LTP may be induced by activation of mAChRs (see Introduction). We tested the effects of the wide-spectrum mAChR antagonist atropine (0.3 μM) that suppressed both the Ca^{2+} wave and the LTP_{IP3}, (data not shown) and of the specific M1 mAChR antagonist pirenzepine (75 nM). Blockade of M1 mAChRs with pirenzepine suppressed the Ca^{2+} wave and the persistent synaptic enhancement normally produced by the ACh puff (Fig. 2*A*). Therefore, EPSCs recorded before and after the ACh challenge were essentially identical ($p > 0.05$ in both cases; $n = 8$) under pirenzepine (Fig. 2*B*). Both atropine and pirenzepine suppressed the initial presynaptic inhibition without modifying control synaptic responses ($p > 0.05$ in both cases; $n = 10$ and $n = 8$, respectively). The long-lasting inward current was also suppressed by atropine, whereas it was insensitive to pirenzepine (data not shown).

Superfusion with the M2 mAChR antagonist methoctramine (1 μM) or with the α-7 nicotinic receptor antagonist MLA (0.1 μM) did not modify the initial presynaptic inhibition, the long-lasting inward current, the LTP_{IP3}, nor the Ca^{2+} wave induced by ACh (Fig. 2*A*,*B*) ($p > 0.05$; $n = 8$). However, when methoctramine was coapplied with pirenzepine, the long-lasting inward current was abolished (data not shown). To completely rule out a possible role of nAChRs, we applied higher doses of MLA (up to 125 μM; $n = 6$), and results were the same as those obtained with the lower doses (data not shown).

The above results are consistent with the initial inhibition, the rise of the intracellular Ca^{2+} signal, and the LTP_{IP3} being exclusively caused by activation of M1 mAChRs.

Both the Ca^{2+} wave and the long-lasting synaptic enhancement are mediated by IP_3

The induction of many forms of long-lasting enhancement (e.g., LTP at SC synapses) requires the activation of NMDARs and Ca^{2+} influx through NMDAR/channels (Malenka et al., 1989; Zucker, 1999). However, inhibition of NMDARs with APV (50 μM) did not modify this synaptic enhancement ($p > 0.05$; $n = 7$) (Fig. 3*A*). In this situation of isolation of the AMPA component of EPSCs ($EPSC_{AMPA}$), the magnitude and time course of the synaptic enhancement induced by the ACh puff were essentially identical to those in control conditions. Pirenzepine also suppressed LTP_{IP3} of the $EPSC_{AMPA}$ isolated under block of NMDARs with APV (50 μM; $p > 0.05$; $n = 6$) (data not shown). Metabotropic glutamate receptors (mGluRs) have been shown to facilitate the induction of LTP (Cohen et al., 1998) and could contribute to this synaptic enhancement. However, MCPG (1 mM), a wide-spectrum mGluR antagonist, did not suppress this synaptic enhancement ($p > 0.05$; $n = 6$) (data not shown). Therefore, this synaptic enhancement does not rely on the activation of NMDARs or mGluRs.

The Ca^{2+} signal and the subsequent LTP_{IP3} were insensitive to blockade of NMDARs with APV (50 μM; $n = 7$; $p > 0.05$) and to intracellular loading with ruthenium red (400 μM RuRed; $n = 7$; $p > 0.05$) that inhibits Ca^{2+} release from ryanodine-sensitive ER

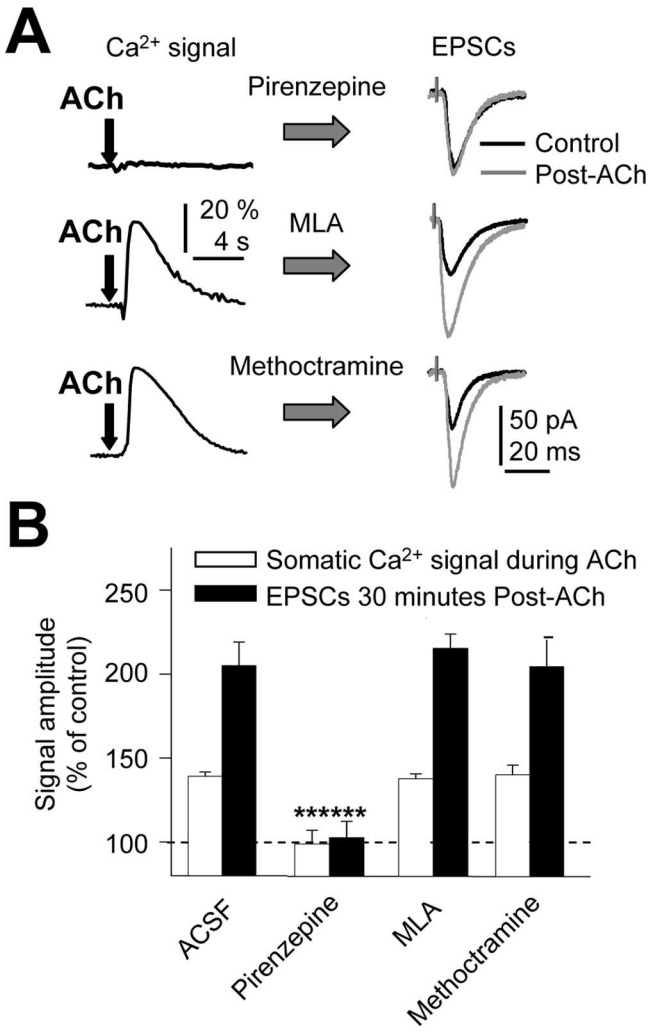

Figure 2. The postsynaptic Ca^{2+} elevation and long-lasting synaptic enhancement require M1 mAChR activation. ***A***, Averaged somatic Ca^{2+} signal induced by ACh and the superimposed EPSCs before (Control; black trace) and after ACh (gray trace) during superfusion with pirenzepine (75 nM), MLA (0.1 μM), and methoctramine (1 μM). ***B***, Summary data showing the ACh effect on the somatic Ca^{2+} signal (white bars) and post-ACh EPSC amplitude (black bars) in control ACSF ($n = 20$) and when pirenzepine ($n = 8$; $p > 0.05$), MLA ($n = 8$; $p < 0.01$), and methoctramine ($n = 8$; $p < 0.01$) were added.

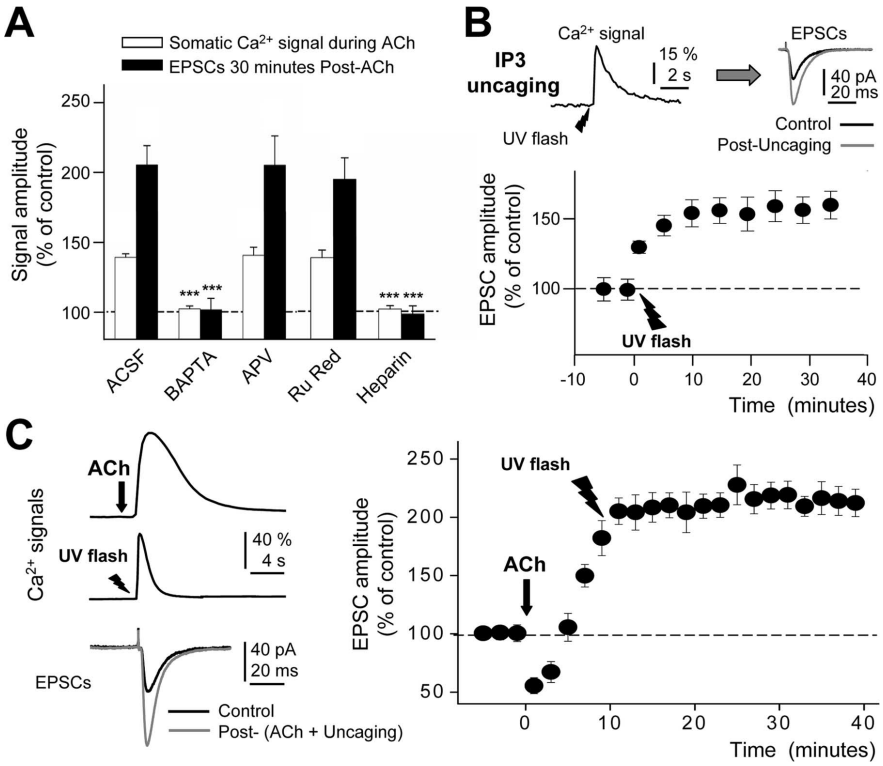

Figure 3. Both the Ca^{2+} wave and the long-lasting synaptic enhancement are mediated by IP_3. ***A***, Summary data showing the ACh effect on the somatic Ca^{2+} signal (white bars) and post-ACh EPSC amplitude (black bars) in control ACSF ($n = 20$), BAPTA (50 mM in the pipette solution; $n = 6$), APV (50 μM; $n = 7$), ruthenium red (400 μM RuRed in the pipette solution; $n = 7$), and heparin (5 mg/ml in the pipette solution; $n = 8$). Note the close relationship between the Ca^{2+} signal and the EPSC potentiation. The LTP_{IP3} induced by ACh is only prevented when the Ca^{2+} signal is blocked with heparin or BAPTA. ***B***, Top, Representative somatic Ca^{2+} signal induced by IP_3 uncaging (100 μM) and superimposed control EPSC (black trace) and 30 min after uncaging (gray trace) during LTP. ***B***, Bottom, Time course of the EPSC amplitude changes (percentage) during the induction of LTP_{IP3} by IP_3 uncaging ($n = 7$). ***C***, Left, Representative Ca^{2+} signals induced by ACh application (5 min after breaking the seal), IP_3 uncaging (10 min later), and superimposed control EPSC (black trace) and 30 min after uncaging (gray trace) during LTP. ***C***, Right, Time course of the EPSC amplitude (percentage) during the induction of LTP_{IP3} by ACh (black arrow; $n = 6$) and by IP_3 uncaging (black ray). Note the occlusion between the potentiation induced by the Ach "puff" and the one induced by IP_3 uncaging.

stores (Fig. 3*A*). A dominant and widespread action of M1 and M3 mAChR activation is the release of Ca^{2+} from IP_3-sensitive ER stores via activation of IP_3Rs (Power and Sah, 2002). Intracellular dialysis with heparin (5 mg/ml), an antagonist of IP_3Rs, suppressed both the Ca^{2+} signal and the LTP_{IP3} (Fig. 3*A*) ($n = 8$; $p > 0.05$). Depletion of Ca^{2+} stores with extracellular thapsigargin (1 μM; $n = 4$; data not shown) and intracellular Ca^{2+} chelation by BAPTA loading (50 mM in the pipette solution) also suppressed the Ca^{2+} signal and the LTP_{IP3} ($n = 6$; $p > 0.05$) (Fig. 3*A*).

Therefore, the above results imply that a rise in intracellular Ca^{2+} released from IP_3-sensitive ER stores preceded and was required for the induction of LTP_{IP3}. In contrast, neither a contribution from ryanodine-sensitive Ca^{2+} stores nor of Ca^{2+} influx through NMDAR/channels were essential to generate LTP_{IP3}.

In view of the above results, we tested the effects of photolysis of caged IP_3 that releases Ca^{2+} from IP_3-sensitive ER stores via direct activation of IP_3Rs without participation of synthesis of IP_3. Uncaging of IP_3 induced a large, brief, synchronous rise in intracellular Ca^{2+} that had a larger magnitude at the soma than the apical dendrite (by 33.1 ± 9.7%; $p < 0.01$; $n = 7$). The Ca^{2+} rise was followed by synaptic enhancement (by 160.2 ± 9.7%; $p < 0.05$; $n = 7$) with characteristics essentially identical to the one induced by ACh puffs (Fig. 3*B*; see supplemental video 2, available at www.jneurosci.org as supplemental material). In contrast, IP_3 uncaging did not induce an inward current (data not shown) and was not preceded by presynaptic inhibition of EPSCs (Fig. 3*B*). Therefore, these results are consistent with a functional relationship between the activation of IP_3-sensitive stores, the subsequent release of Ca^{2+}, and the induction of the LTP_{IP3}. In addition, these results suggest that neither depolarization nor the initial presynaptic inhibition are required for the induction of LTP_{IP3}.

We also analyzed the possible occlusion between the LTP_{IP3} induced by the ACh puff and that generated by the uncaging of IP_3. We loaded cells with the caged IP_3 and recorded a control stable baseline EPSC during the first 5 min after breaking the seal. An ACh puff was then delivered to induce the LTP_{IP3}, and 10 min later, when the EPSC amplitude had increased (205.2 ± 15.6% of controls; $p < 0.001$; $n = 6$), we flashed the loaded cell to uncage the IP_3. The IP_3 uncaging did not modify the LTP_{IP3} induced by the ACh puff (215.2 ± 17.6% of controls; $p > 0.05$; $n = 6$) (Fig. 3*C*). These results imply an occlusion between both methods of LTP induction, suggesting that they share common postsynaptic mechanisms where activation of IP_3Rs is required.

Finally, to determine whether the LTP_{IP3} was present at more physiological temperatures, we repeated the above analysis at 32°C. ACh induced similar postsynaptic Ca^{2+} elevations and long-lasting enhancements of synaptic transmission that were blocked by pirenzepine at the higher temperature of 32°C. In addition, IP_3 uncaging also induced the LTP_{IP3} at 32°C (see supplemental Fig. 1, available at www.jneurosci.org as supplemental material), suggesting that similar mechanisms could be present in the natural condition.

LTP_{IP3} is paralleled by an increased expression of AMPARs in dendritic spines

Changes in postsynaptic responsiveness to presynaptically released glutamate might be mediated by a change in AMPAR number at the postsynaptic membrane (Malinow and Malenka, 2002). To determine whether AMPARs are inserted during the cholinergically induced LTP_{IP3}, we analyzed the effect of ACh on the content of recombinant AMPAR at the surface of spines of CA1 pyramidal neurons (Fig. 4). We expressed GluR1 or GluR2 tagged with the SEP, a pH-sensitive form of green fluorescence protein that marks surface AMPA receptors (Ashby et al., 2004; Kopec et al., 2006) using a Sindbis virus. CA1 pyramidal neurons infected with Sindbis virus-expressing GluR1-SEP subunit and t-dimer red protein were visualized before (control) and 30 min after ACh application (post-ACh) using the two-photon microscope (Fig. 4*A*). ACh induced an increase in the spine green fluorescence signal (133.9 ± 8.0%; $p < 0.001$; $n = 145$ spines, 8 cells) without significant changes in the spine red signal (112.2 ± 8.2%; $p > 0.05$; same cells) nor in the red and green dendritic

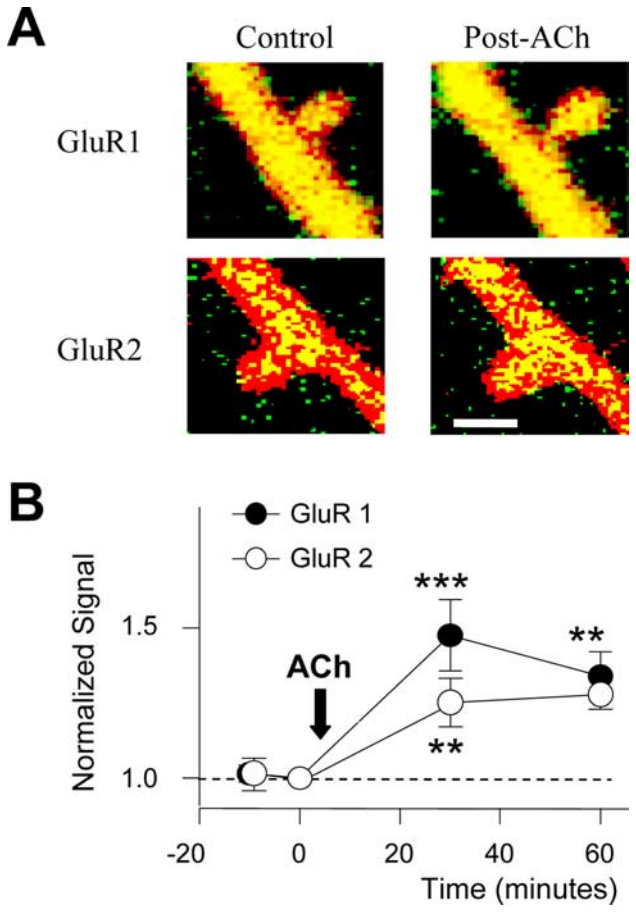

Figure 4. ACh causes insertion of AMPARs in dendritic spines. ***A***, Images of representative spines, expressing GluR1-SEP (top), GluR2-SEP (bottom), and t-dimer red protein, before (Control) and after ACh. Scale bar, 1 μm. Note the increase in the yellow signal 30 min after application of ACh in both GluR1- and GluR2-expressing spines without changes in spine volume. ***B***, Summary data showing the ACh effect on the content of GluR1 (black circles; $n = 145$ spines, 8 cells; $p < 0.001$) and GluR2 (white circles; $n = 75$ spines, 6 cells; $p < 0.01$) on the spines.

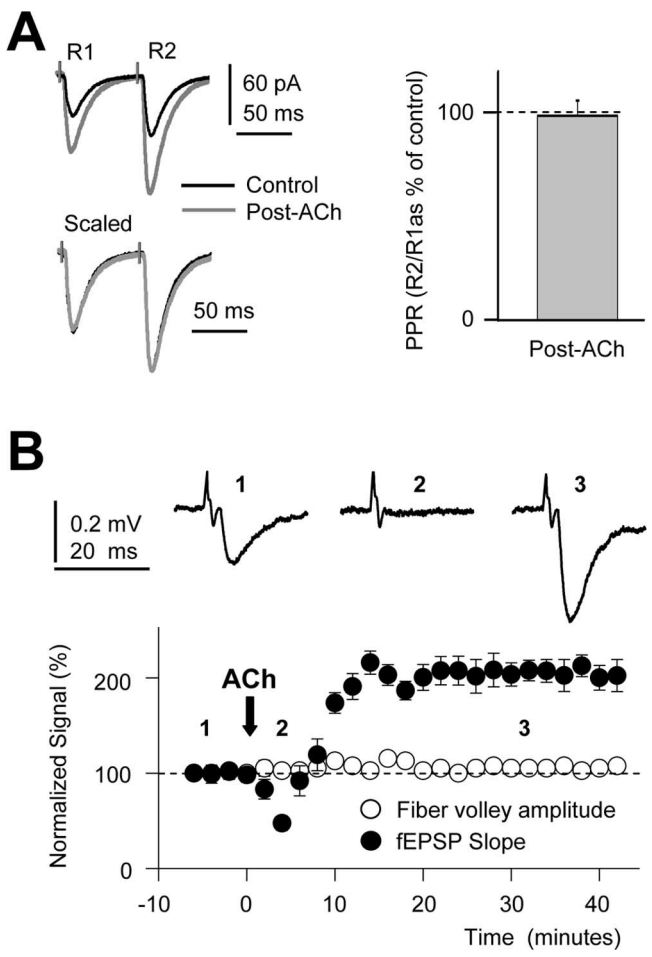

Figure 5. Absence of presynaptic contribution to the LTP_{IP3}. ***A***, Left, Superimposed representative EPSCs evoked by paired pulse stimulation before (control; black trace) and after ACh (gray trace) and the EPSCs scaled to show the lack of modification in the PPR. ***A***, Right, Summary data ($n = 15$) showing the PPR (R2/R1; as a percentage of control). ***B***, Top, Representative averaged extracellular responses before (1), 3 min after ACh (2), and ~30 min after ACh (3). Note the absence of modification of the fiber volley. ***B***, Bottom, Time course of the fEPSP slope (black circles) and fiber volley amplitude (white circles) during the initial inhibition and subsequent LTP_{IP3} after the ACh puff (black arrow; $n = 15$).

fluorescence signal ($p > 0.05$), indicating an increase of new GluR1 AMPARs at the spine surface without changes in the spine volume (Fig. 4*B*). Moreover, in similar experiments using the GluR2-SEP subunit, ACh induced an increase of GluR2 AMPARs at the spine surface (spine green fluorescence signal, 128.6 ± 5.12%; $p < 0.01$; $n = 75$ spines, 6 cells) (Fig. 4*B*) without significant changes in the spine or dendrite red signal, nor in the dendrite green signal ($p > 0.05$; same cells). Therefore, ACh induced the insertion of both GluR1 and GluR2 AMPARs at the spine surface of CA1 pyramidal neurons.

Together the above results suggest that the LTP_{IP3} induced by the ACh puff was caused by an increase in the number of AMPARs expressed at the spines of CA1 pyramidal neurons.

Absence of presynaptic contribution to the LTP_{IP3}

We analyzed whether LTP_{IP3} had a presynaptic component (Castillo et al., 2002) analyzing the changes in PPRs that are a sign of modifications in the release probability of the presynaptic terminal (Zucker, 1999; Fernandez de Sevilla et al., 2002; Oertner et al., 2002). Control PPRs were characterized by paired-pulse facilitation in which the second EPSC (R2) was larger than the first (R1), indicating that the group of stimulated synapses had on the average a low release probability. There were no modifications of the PPR with LTP_{IP3} ($p > 0.05$; $n = 15$) (Fig. 5*A*), consistent with the lack of a presynaptic contribution. However, during the initial presynaptic inhibition, there was a transient increase in the PPR (data not shown) reflecting the decrease in the release probability as a result of the activation of presynaptic mAChRs (Fernandez de Sevilla et al., 2002; Cabezas and Buno, 2006).

A possible increase in the excitability of the SC axons, leading to an increased number of SC axons recruited by a stimulating electrode, could account for the increased synaptic transmission induced by the ACh puff. To test this possibility, we recorded extracellularly the fiber volley and the fEPSP evoked by SC stimulation before, during, and 30 min after the ACh puff applied close to the recording electrode (~250 μm) at the stratum pyramidal–radiatum border (Fig. 5*B*, Control, during ACh, and Post-ACh, respectively). The fEPSP slope was initially reduced (47.5 ± 7.4%; $p < 0.001$; $n = 15$) and later potentiated (207.3 ± 11.9%; $p < 0.001$; $n = 15$) by the ACh puff; in contrast, the fiber volley, which records the number of presynaptic fibers activated, remained unaltered throughout the experiment ($p > 0.5$; $n = 15$) (Fig. 5*B*).

Together these results suggest that LTP_{IP3} is exclusively mediated through postsynaptic mechanisms. LTP_{IP3} persisted up to

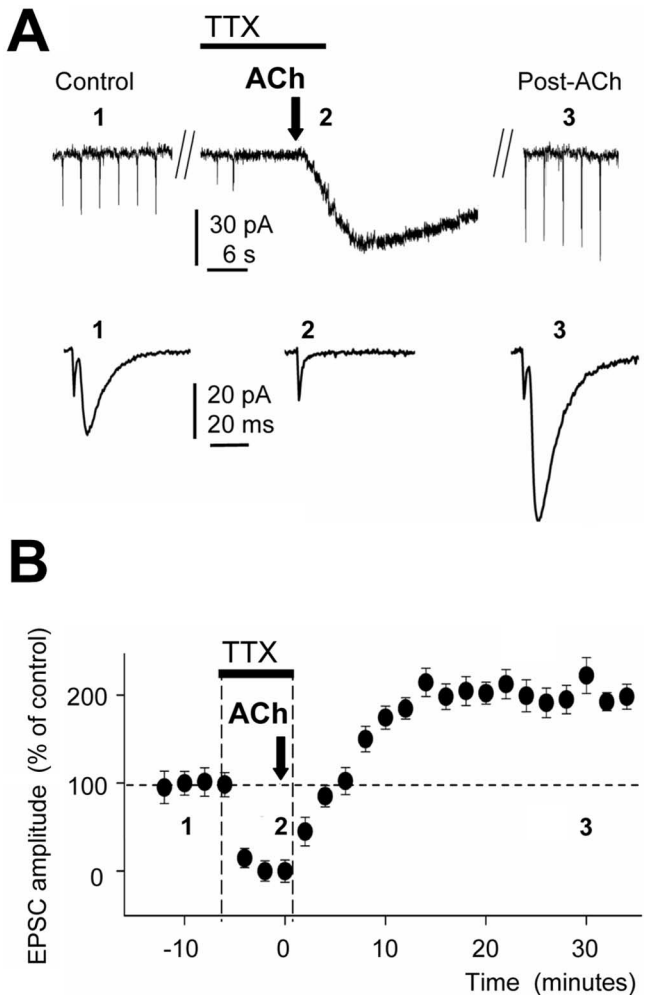

Figure 6. LTP_{IP3} does not require presynaptic and postsynaptic action potentials. ***A***, Top, Representative recording showing the EPSCs in control (1), their absence after blockade of sodium channels with TTX (100 nM), and the slow inward current evoked by ACh application (2). Note the sustained EPSC potentiation recorded after 30 min of TTX washout (3; Post-ACh). ***A***, Bottom, EPSCs recorded at 1, 2, and 3. ***B***, Time course of the EPSC amplitude (percentage) during TTX, the induction of LTP_{IP3} by ACh (black arrow; $n = 10$), and washout in control solution.

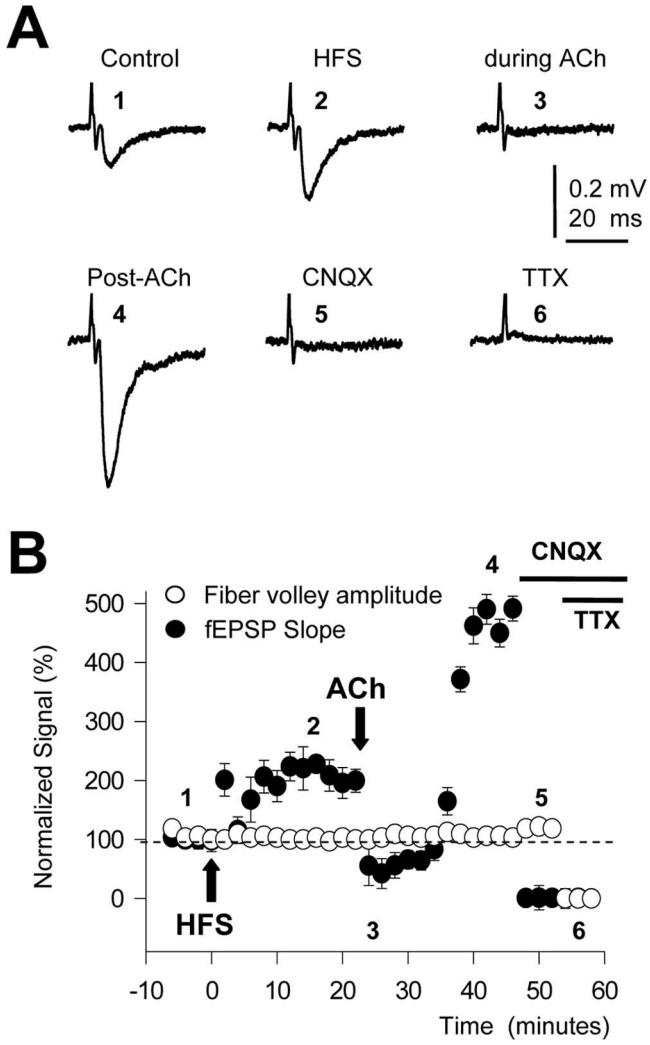

Figure 7. LTP_{IP3} and LTP_H can be superimposed. ***A***, Representative extracellular recordings in control (1), after HFS of SCs (2), after an ACh puff (3), and during LTP_{IP3} (4). The effects of blockade of $EPSC_{AMPA}$ with 20 μM CNQX (5) and of voltage-gated Na^+ conductances by 100 nM TTX (6) are also shown. ***B***, Time course of the fEPSP slope and fiber volley amplitude (filled and open circles, respectively) in control (1), during the LTP_H (2) induced by HFS and the LTP_{IP3} (4) induced by an ACh puff, and during CNQX (5) and TTX (6; $n = 6$).

4 h, a duration that is similar to the LTP induced by classical HFS of SCs (Malenka and Bear, 2004) (see supplemental Fig. 1, available at www.jneurosci.org as supplemental material).

LTP_{IP3} does not require correlated AP activity

A property that typifies the induction of the classical LTP, the "Hebbian principle" (LTP_H), is the need for correlated presynaptic and postsynaptic action potential (AP) activity. Therefore, to identify whether this rule was applicable to this form of LTP, we inhibited voltage-gated Na^+ channels with TTX (100 nM), which blocks both presynaptic and postsynaptic APs and prevents evoked and spontaneous synaptic activity (Fig. 6*A*,*B*). When SC EPSCs and postsynaptic APs (tested with brief depolarizing pulses) had disappeared, we applied the ACh puff. The typical long-lasting inward current (Fig. 6*A*) and Ca^{2+} signal were evoked by the ACh puff (data not shown). After TTX washout, the EPSC gradually recovered, and ~25 min later, a strong LTP_{IP3} was induced (by 201.3 ± 8.5%; $p < 0.001$; $n = 10$). A similar superfusion of TTX in control conditions in the absence of the ACh challenge did not modify EPSCs after a washout (data not shown; $p > 0.05$; $n = 6$). These results indicate that inhibition of voltage-gated Na^+ channels and of presynaptic and postsynaptic AP activity did not contribute to LTP_{IP3}.

LTP_{IP3} and LTP_H can be superimposed

The possible interactions between LTP_{IP3} and the classical homosynaptic LTP_H induced by HFS could have important functional implication. With extracellular recordings of fEPSPs that preserve the intracellular mechanisms required to induce the LTP otherwise dialyzed during prolonged whole-cell recordings, we induced LTP_H by stimulating a group of SCs with 30 barrages (50 Hz, 1 s) at 0.5 Hz. When LTP_H had stabilized ~25 min later (at 209.1 ± 25.1% of control values; $p < 0.001$; $n = 6$), we applied an ACh puff as described above (Fig. 7*B*, filled circles). The ACh puff first evoked the initial presynaptic inhibition of the fEPSPs, but of much longer duration (~10 min) than that observed in the absence of a previous LTP_H. The inhibition was followed by an LTP_{IP3} that reached values of 490.1 ± 25.8% of controls ($p < 0.001$; $n = 6$). The first LTP induction protocol enhanced fEPSP slopes by ~200%, and the second augmented fEPSPs an extra ~200%, the LTP reaching a final value of ~400%. Although in

these experiments LTP_H was not saturated, we can conclude that within the amplitudes analyzed both types of LTP tended to add linearly. We checked that the presynaptic fiber volley remained unchanged throughout the recording and when fEPSPs were inhibited with CNQX (20 μM). Finally, we applied 100 nM TTX that completely blocked the presynaptic fiber volley (Fig. 7*B*, open circles).

Therefore, the classical homosynaptic LTP_H and LTP_{IP3} can be superimposed. LTP_{IP3} may serve to ensure an increased synaptic efficacy not requiring activation of glutamatergic synapses and therefore not restricted to the activated synapses but localized close to the site at which mAChRs were activated. In contrast, LTP_H requires the activation of glutamatergic synapses and is restricted to the activated synapses. Therefore, the two regulatory mechanisms may coexist and perform different functions in the same neurons.

An atropine-sensitive long-lasting synaptic enhancement can be induced *in vivo* by stimulation of the medial septum

We tested the effects of tetanic stimulation of medial septum cholinergic neurons on CA1 fEPSPs evoked by SC stimulation. The averaged fEPSP recorded in control conditions showed stable onset slopes throughout SC stimulation at 0.5 Hz during 70 min (Fig. 8*C*). Tetanic stimulation of the medial septum with three 500-ms-duration pulse barrages of 100 μA, 0.3 ms pulses at 100 Hz presented every 2 s increased the SC fEPSP slope (Fig. 8*B*). The facilitation of the fEPSP slope was maximal 5 min after tetanic stimulation and was stable (210 ± 19.9% of controls; $p < 0.01$; $n = 6$) for the remainder of the experiment that lasted up to 60 min (Fig. 8*C*), a result consistent with the properties of an LTP (Malenka and Bear, 2004). To determine whether the LTP induced by the tetanic stimulation of the medial septum was mediated via activation of mAChRs, atropine was applied (5 mg/kg, i.p.) 10 min before the medial septum stimulation. In these conditions a modest facilitation of the SC fEPSP slope of 130.5 ± 11.2% was evoked (Fig. 8*C*) ($p < 0.05$; $n = 6$). The reported brief and transient reduction of synaptic efficacy that followed septal stimuli during *in vivo* experiments (Rovira et al., 1983) was not observed in our study, most likely because this depression lasts <20 s, and its amplitude is at most 20% of the control fEPSP amplitude. Therefore, although possibly present in our experiments, the inhibition remained undetected because we averaged 1 min epochs, which possibly include the onset of LTP, thus canceling out the inhibition. Another possible explanation for the absence of transient depression in our experiments may arise from the slightly different septal stimulation protocols used by Rovira et al. (1983) (15 trains at 1/s of 10 pulses at 100 Hz) and by our group (3 trains at 1/2 s of 50 pulses at 100 Hz).

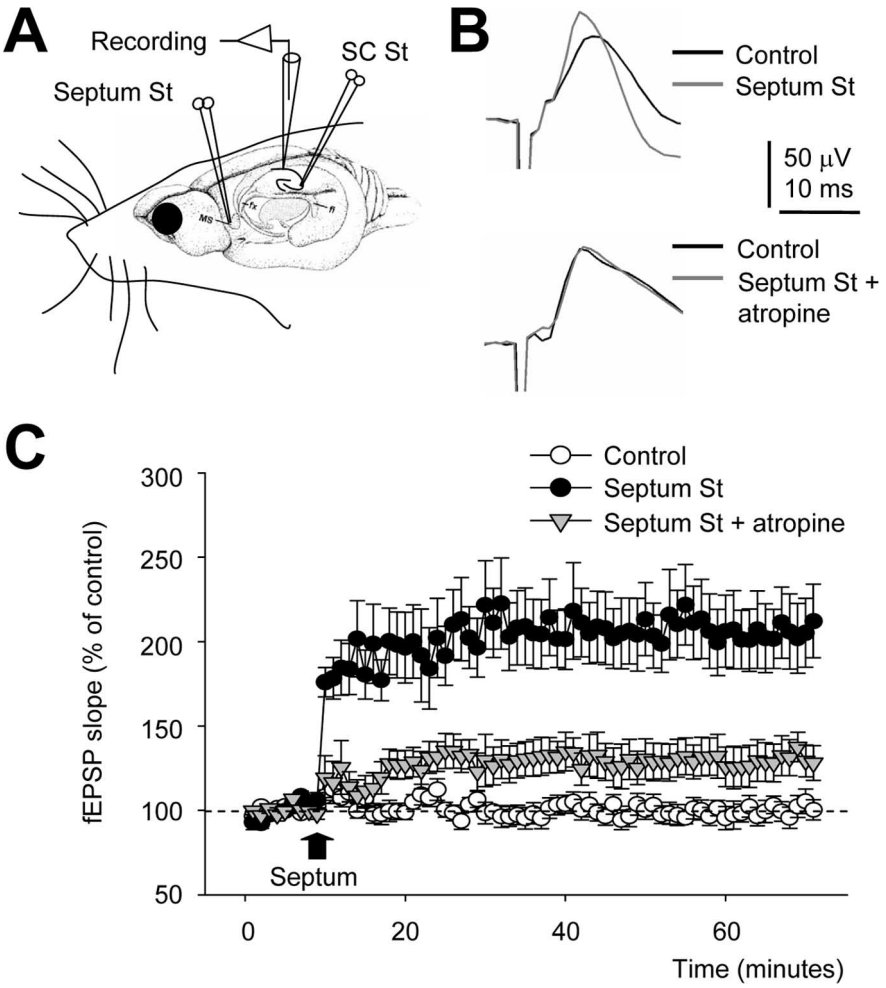

Figure 8. An atropine-sensitive long-lasting synaptic enhancement induced *in vivo* by stimulation of the medial septum. ***A***, Schematic diagram of the experimental setup showing a stimulating electrode placed in the septum (Septum St), another stimulating electrode placed in the CA3 region (SC St), and the recording electrode placed in the CA1 region (Recording). ***B***, Top, Representative extracellular recordings in control (black trace) and after stimulation of the medial septum (gray trace). ***B***, Bottom, Same as top, but under atropine (5 mg/kg). ***C***, Time course of the fEPSP slope (percentage) in control (white circles), when septum is stimulated (black circles), and when septum is stimulated under atropine (gray triangles; $n = 6$).

Discussion

We describe novel mechanisms that mediate a long-lasting synaptic enhancement or LTP_{IP3} that is triggered both by a brief ACh puff applied at the apical dendrite and by stimulation of cholinergic septohippocampal afferents. LTP_{IP3} is expressed postsynaptically and requires the activation of M1 mAChRs, production of IP_3, and release of Ca^{2+} from IP_3-sensitive stores by the activation of IP_3Rs. LTP_{IP3} does not need activation of NMDARs, does not comply with the "Hebbian" principle, and can be induced *in vivo* by tetanic stimulation of the medial septum.

A potentiation of SC EPSPs induced by carbachol (CCh) has been described by Auerbach and Segal (1994, 1996). In contrast with our results, the potentiation described by those authors was mediated via activation of M2 mAChRs and mainly caused by an enhancement of an NMDA component. The discrepancy between our results and those of Auerbach and Segal (1994, 1996) could reside in the prolonged presence of CCh in their case that may have stimulated both intracellular and circuit mechanisms not activated by the transient localized pulses of ACh used by us. Another possible cause is that muscarinic innervation of CA1 pyramidal cells changes markedly during development (Amenta

et al., 1995), and the rats used by Auerbach and Segal were much older (>7 weeks and up to 36 months) than our sample (14–16 d). A specific potentiation of the NMDA component induced by ACh and mediated by M2 mAChRs and IP_3 production has also been reported (Markram and Segal, 1990). This potentiation is also different from the LTP_{IP3} reported here because it is short-lived and required activation of NMDARs. Higher CCh concentrations than those used by Auerbach and Segal (1994, 1996) may induce long-term depression (LTD) in the rat visual cortex and hippocampus *in vitro* via activation of M1 mAChRs (Kirkwood et al., 1999; Scheiderer et al., 2006). However, in contrast to the LTP_{IP3}, this LTD requires activation of NMDARs and correlated presynaptic and postsynaptic activity.

We show that the LTP_{IP3} is closely linked to the genesis of Ca^{2+} waves in the apical dendrites of CA1 pyramidal cells and that BAPTA loading, intracellular heparin, and thapsigargin, which inhibit Ca^{2+} waves and the increase of the intracellular Ca^{2+} concentration, suppress LTP_{IP3}. In contrast, inhibition of Ca^{2+} release from ryanodine-sensitive ER stores with ruthenium red and inhibition of Ca^{2+} influx by inhibiting NMDARs with APV did not interfere with the Ca^{2+} signals, nor with LTP_{IP3}. Moreover, LTP_{IP3} does not require membrane depolarization or Ca^{2+} influx through voltage-gated Ca^{2+} channels because both are absent in the LTP_{IP3} induced by IP_3 uncaging. Therefore, the intracellular Ca^{2+} elevations required to induce this form of LTP were via Ca^{2+} release from IP_3-sensitive ER stores.

The ER itself is thought to extend to all parts of the dendritic arbor and spines in Purkinje and CA1 pyramidal neurons (Spacek and Harris, 1997). These localizations agree with the sites that express IP_3Rs in those cells (Sharp et al., 1993). ACh puffs triggered dendrosomatic Ca^{2+} waves with a delay, whereas IP_3 uncaging produced a rapid synchronous Ca^{2+} elevation at the apical dendritic shaft and soma. The limiting factor in the delay between the ACh puff and the Ca^{2+} rise could be the time required for the production of IP_3, whereas the activation of mAChRs and IP_3Rs and the subsequent Ca^{2+} release contribute less to the delay. In addition, the differences between puffs and uncaging could indicate that Ca^{2+} waves induced by ACh puffs are not determined by the distribution of IP_3R over the ER nor by the localization of membrane mAChRs (Bardo et al., 2006). The site of origin of the Ca^{2+} waves far from the ACh application site could be caused by the positive interaction between IP_3 and Ca^{2+} occurring at sites where IP_3 induced larger Ca^{2+} elevations (Mak et al., 2001).

The cholinergic innervation of the CA1 region originates both from extrinsic and intrinsic cholinergic neurons (Frotscher and Leranth, 1985; Frotscher et al., 2000). In the CA1 region, cholinergic afferents terminate both on pyramidal cells and interneurons, acting mainly through muscarinic receptors in the former and nicotinic receptors in the latter (Amenta et al., 1995). Although there is widespread expression of mAChRs, particularly of the M1 subtype, in both neuronal soma and dendrites in rat hippocampal pyramidal cells (Levey et al., 1995; Power and Sah, 2002), there is also controversy regarding the contribution of the mAChR type to the different muscarinic actions in the CA1 region (Dutar and Nicoll, 1988; Ovsepian et al., 2004; Shinoe et al., 2005).

Interestingly, several neurotransmitters can enhance receptor-mediated activation of PLC and IP_3 production. Release from IP_3-sensitive stores, Ca^{2+} waves, and facilitation of LTP in hippocampal pyramidal cells can be induced by mGluRs activation (Cohen et al., 1998), possibly acting through intracellular cascades similar to those activated by mAChRs. Purinergic and adrenergic receptors also activate IP_3 production (Nishizaki and Mori, 1998). Therefore, different membrane receptors may activate the same intracellular signaling cascade. However, it remains to be determined what functional demands require signaling through the different membrane receptors to produce IP_3 and the induction of enduring modifications in synaptic efficacy.

AMPAR expression at the postsynaptic membrane is highly dynamic (Malinow and Malenka, 2002; Song and Huganir, 2002; Bredt and Nicoll, 2003). The rapid mobility of AMPARs occurs in a constitutive manner, with continual turnover of AMPARs at the synaptic membrane mediated by exocytosis and endocytosis (Lin et al., 2000), as well as through lateral mobility (Triller and Choquet, 2005). However, AMPAR trafficking is also modified by synaptic activity (Lissin et al., 1999; Ehlers, 2000; Lin et al., 2000). These activity-dependent changes in AMPAR trafficking have been linked to the modulation of synaptic strength that occurs during some forms of LTP and LTD (Malinow and Malenka, 2002). Our data demonstrate that ACh induces the increase of both GluR1 and GluR2 subunits of the AMPARs at the spines of CA1 pyramidal neurons. However we cannot discard a possible increase in the conductance of preexisting surface-expressed receptors (Benke et al., 1998) as a mechanism contributing to the long-lasting increase in the $EPSC_{AMPA}$.

In conclusion, this LTP_{IP3} is expressed postsynaptically and requires Ca^{2+} release from IP_3-sensitive stores and a rise in intracellular Ca^{2+} concentration. In contrast, it does not require depolarization or activation of voltage-gated Ca^{2+} conductances, nor of NMDARs that are indispensable to induce the classical LTP_H. In addition, a similar muscarinic long-lasting enhancement of SC EPSPs may be induced by tetanic stimulation of septohippocampal cholinergic fibers, suggesting that LTP_{IP3} may be functional in the natural condition. This view is consistent with the high firing rates of medial septal neurons *in vivo* (Gogolak et al., 1968; Gaztelu and Buno, 1982). This novel LTP_{IP3} indicates that sustained modifications of synaptic efficacy may be more diverse than previously considered and reveals yet another cascade of postsynaptic events that might be present during behavior and can drive AMPARs into synapses and enhance synaptic transmission exclusively through Ca^{2+} release from ER stores.

References

Abe T, Sugihara H, Nawa H, Shigemoto R, Mizuno N, Nakanishi S (1992) Molecular characterization of a novel metabotropic glutamate receptor mGluR5 coupled to inositol phosphate/Ca2+ signal transduction. J Biol Chem 267:13361–13368.

Aigner TG (1995) Pharmacology of memory: cholinergic-glutamatergic interactions. Curr Opin Neurobiol 5:155–160.

Amenta F, Liu A, Giannella M, Pigini M, Tayebati SK, Zaccheo D (1995) Age-related changes in the density of muscarinic cholinergic M1 and M2 receptor subtypes in pyramidal neurons of the rat hippocampus. Eur J Histochem 39:107–116.

Ashby MC, Ibaraki K, Henley JM (2004) It's green outside: tracking cell surface proteins with pH-sensitive GFP. Trends Neurosci 27:257–261.

Auerbach JM, Segal M (1994) A novel cholinergic induction of long-term potentiation in rat hippocampus. J Neurophysiol 72:2034–2040.

Auerbach JM, Segal M (1996) Muscarinic receptors mediating depression and long-term potentiation in rat hippocampus. J Physiol 492:479–493.

Bardo S, Cavazzini MG, Emptage N (2006) The role of the endoplasmic reticulum Ca2+ store in the plasticity of central neurons. Trends Pharmacol Sci 27:78–84.

Benke TA, Luthi A, Isaac JT, Collingridge GL (1998) Modulation of AMPA receptor unitary conductance by synaptic activity. Nature 393:793–797.

Blokland A (1995) Acetylcholine: a neurotransmitter for learning and memory? Brain Res Brain Res Rev 21:285–300.

Borde M, Cazalets JR, Buno W (1995) Activity-dependent response depression in rat hippocampal CA1 pyramidal neurons in vitro. J Neurophysiol 74:1714–1729.

Bredt DS, Nicoll RA (2003) AMPA receptor trafficking at excitatory synapses. Neuron 40:361–379.

Cabezas C, Buno W (2006) Distinct transmitter release properties determine differences in short-term plasticity at functional and silent synapses. J Neurophysiol 95:3024–3034.

Castillo PE, Schoch S, Schmitz F, Sudhof TC, Malenka RC (2002) RIM1alpha is required for presynaptic long-term potentiation. Nature 415:327–330.

Cohen AS, Raymond CR, Abraham WC (1998) Priming of long-term potentiation induced by activation of metabotropic glutamate receptors coupled to phospholipase C. Hippocampus 8:160–170.

Dudar JD (1977) The role of the septal nuclei in the release of acetyl-choline from the rabbit cerebral cortex and dorsal hippocampus and the effect of atropine. Brain Res 129:237–246.

Dutar P, Nicoll RA (1988) Classification of muscarinic responses in hippocampus in terms of receptor subtypes and second-messenger systems: electrophysiological studies *in vitro*. J Neurosci 8:4214–4224.

Ehlers MD (2000) Reinsertion or degradation of AMPA receptors determined by activity-dependent endocytic sorting. Neuron 28:511–525.

Fernandez de Sevilla D, Buno W (2003) Presynaptic inhibition of Schaffer collateral synapses by stimulation of hippocampal cholinergic afferent fibres. Eur J Neurosci 17:555–558.

Fernandez de Sevilla D, Cabezas C, de Prada AN, Sanchez-Jimenez A, Buno W (2002) Selective muscarinic regulation of functional glutamatergic Schaffer collateral synapses in rat CA1 pyramidal neurons. J Physiol (Lond) 545:51–63.

Frotscher M, Leranth C (1985) Cholinergic innervation of the rat hippocampus as revealed by choline acetyltransferase immunocytochemistry: a combined light and electron microscopic study. J Comp Neurol 239:237–246.

Frotscher M, Vida I, Bender R (2000) Evidence for the existence of non-GABAergic, cholinergic interneurons in the rodent hippocampus. Neuroscience 96:27–31.

Gaztelu JM, Buno Jr W (1982) Septo-hippocampal relationships during EEG theta rhythm. Electroencephalogr Clin Neurophysiol 54:375–387.

Gogolak G, Stumpf C, Petsche H, Sterc J (1968) The firing pattern of septal neurons and the form of the hippocampal theta wave. Brain Res 7:201–207.

Hasselmo ME (1999) Neuromodulation: acetylcholine and memory consolidation. Trends Cogn Sci 3:351–359.

Hoffman DA, Sprengel R, Sakmann B (2002) Molecular dissection of hippocampal theta-burst pairing potentiation. Proc Natl Acad Sci USA 99:7740–7745.

Huerta PT, Lisman JE (1995) Bidirectional synaptic plasticity induced by a single burst during cholinergic theta oscillation in CA1 in vitro. Neuron 15:1053–1063.

Kirkwood A, Rozas C, Kirkwood J, Perez F, Bear MF (1999) Modulation of long-term synaptic depression in visual cortex by acetylcholine and norepinephrine. J Neurosci 19:1599–1609.

Kopec CD, Li B, Wei W, Boehm J, Malinow R (2006) Glutamate receptor exocytosis and spine enlargement during chemically induced long-term potentiation. J Neurosci 26:2000–2009.

Levey AI, Edmunds SM, Koliatsos V, Wiley RG, Heilman CJ (1995) Expression of m1–m4 muscarinic acetylcholine receptor proteins in rat hippocampus and regulation by cholinergic innervation. J Neurosci 15:4077–4092.

Lin JW, Ju W, Foster K, Lee SH, Ahmadian G, Wyszynski M, Wang YT, Sheng M (2000) Distinct molecular mechanisms and divergent endocytotic pathways of AMPA receptor internalization. Nat Neurosci 3:1282–1290.

Lissin DV, Carroll RC, Nicoll RA, Malenka RC, von Zastrow M (1999) Rapid, activation-induced redistribution of ionotropic glutamate receptors in cultured hippocampal neurons. J Neurosci 19:1263–1272.

Mak DO, McBride S, Foskett JK (2001) Regulation by Ca2+ and inositol 1,4,5-trisphosphate (InsP3) of single recombinant type 3 InsP3 receptor channels. Ca2+ activation uniquely distinguishes types 1 and 3 insp3 receptors. J Gen Physiol 117:435–446.

Malenka RC, Bear MF (2004) LTP and LTD: an embarrassment of riches. Neuron 44:5–21.

Malenka RC, Kauer JA, Perkel DJ, Nicoll RA (1989) The impact of postsynaptic calcium on synaptic transmission–its role in long-term potentiation. Trends Neurosci 12:444–450.

Malinow R, Malenka RC (2002) AMPA receptor trafficking and synaptic plasticity. Annu Rev Neurosci 25:103–126.

Markram H, Segal M (1990) Acetylcholine potentiates responses to *N*-methyl-D-aspartate in the rat hippocampus. Neurosci Lett 113:62–65.

Markram H, Helm PJ, Sakmann B (1995) Dendritic calcium transients evoked by single back-propagating action potentials in rat neocortical pyramidal neurons. J Physiol 485:1–20.

Nishizaki T, Mori M (1998) Diverse signal transduction pathways mediated by endogenous P2 receptors in cultured rat cerebral cortical neurons. J Neurophysiol 79:2513–2521.

Oertner TG, Sabatini BL, Nimchinsky EA, Svoboda K (2002) Facilitation at single synapses probed with optical quantal analysis. Nat Neurosci 5:657–664.

Ovsepian SV, Anwyl R, Rowan MJ (2004) Endogenous acetylcholine lowers the threshold for long-term potentiation induction in the CA1 area through muscarinic receptor activation: in vivo study. Eur J Neurosci 20:1267–1275.

Paxinos G, Watson C (1986) The rat brain in stereotaxic coordinates. New York: Academic.

Power JM, Sah P (2002) Nuclear calcium signaling evoked by cholinergic stimulation in hippocampal CA1 pyramidal neurons. J Neurosci 22:3454–3462.

Qian J, Saggau P (1997) Presynaptic inhibition of synaptic transmission in the rat hippocampus by activation of muscarinic receptors: involvement of presynaptic calcium influx. Br J Pharmacol 122:511–519.

Ramón y Cajal S (1891) Significación fisiológica de las expansions protoplásmicas y nerviosas de la sustancia gris. Revista de Ciencias Médicas de Barcelona 22:23.

Rose CR, Konnerth A (2001) Stores not just for storage. intracellular calcium release and synaptic plasticity. Neuron 31:519–522.

Rovira C, Ben-Ari Y, Cherubini E (1983) Dual cholinergic modulation of hippocampal somatic and dendritic field potentials by the septo-hippocampal pathway. Exp Brain Res 49:151–155.

Scheiderer CL, McCutchen E, Thacker EE, Kolasa K, Ward MK, Parsons D, Harrell LE, Dobrunz LE, McMahon LL (2006) Sympathetic sprouting drives hippocampal cholinergic reinnervation that prevents loss of a muscarinic receptor-dependent long-term depression at CA3–CA1 synapses. J Neurosci 26:3745–3756.

Sharp AH, McPherson PS, Dawson TM, Aoki C, Campbell KP, Snyder SH (1993) Differential immunohistochemical localization of inositol 1,4,5-trisphosphate- and ryanodine-sensitive Ca^{2+} release channels in rat brain. J Neurosci 13:3051–3063.

Shinoe T, Matsui M, Taketo MM, Manabe T (2005) Modulation of synaptic plasticity by physiological activation of M1 muscarinic acetylcholine receptors in the mouse hippocampus. J Neurosci 25:11194–11200.

Song I, Huganir RL (2002) Regulation of AMPA receptors during synaptic plasticity. Trends Neurosci 25:578–588.

Spacek J, Harris KM (1997) Three-dimensional organization of smooth endoplasmic reticulum in hippocampal CA1 dendrites and dendritic spines of the immature and mature rat. J Neurosci 17:190–203.

Triller A, Choquet D (2005) Surface trafficking of receptors between synaptic and extrasynaptic membranes: and yet they do move! Trends Neurosci 28:133–139.

Valentino RJ, Dingledine R (1981) Presynaptic inhibitory effect of acetylcholine in the hippocampus. J Neurosci 1:784–792.

Zenchenko KI, Kokoz YM, Ivanov VT, Ziganshin RH, Vinogradova OS (2000) State-dependent effects of some neuropeptides and neurotransmitters on neuronal activity of the medial septal area in brain slices of the ground squirrel, *Citellus undulatus*. Neuroscience 96:791–805.

Zucker RS (1999) Calcium- and activity-dependent synaptic plasticity. Curr Opin Neurobiol 9:305–313.